Materials Research Proceedings 41 (2024) 2365-2373 https://doi.org/10.21741/9781644903131-260

Experimental derivation of process input parameters for electrochemical precision machining of a powder metallurgical tool steel

PETERMANN Richard[1,a *], CLAUß Pascal[1,b], DAMM Philipp[1,c], MEICHSNER Gunnar[1,d] and HACKERT-OSCHÄTZCHEN Matthias[1,e]

[1]Chair of Manufacturing Technology with Focus Machining, Faculty of Mechanical Engineering, Otto von Guericke University Magdeburg, Universitätsplatz 2, 39106 Magdeburg, Germany

[a]richard.petermann@ovgu.de, [b]pascal.clauss@ovgu.de, [c]philipp.damm@ovgu.de, [d]gunnar.meichsner@ovgu.de, [e]matthias.hackert-oschaetzchen@ovgu.de

Keywords: Anodic Dissolution, Electrochemical Precision Machining (PECM), Removal Rate, DIN SPEC 91399

Abstract. Powder metallurgical steels are used for tools because of their properties, such as toughness, wear resistance and hardness. During the machining of the tool, the material is hardened. Consequently, the subsequent finishing of the tool is a challenge, as conventional manufacturing processes reach their limit of machinability due to the hardness. An alternative manufacturing technology is electrochemical precision machining (PECM). The PECM process, which is based on anodic metal dissolution, can be applied to machine metallic materials without force, cracks or burrs, regardless of their hardness [1]. Due to the process principle, the mechanical properties of the workpiece are not changed. As a result, the PECM process is suitable for finish machining of tools and finishing of tools. A significant challenge for PECM is the material-specific removal functions [2]. In this paper, the material removal functions of the hardened powder metallurgical steel S390 [3] are analyzed using experimental tests and the achievable surface quality is shown. Subsequently, process input parameters for electrochemical precision machining of S390 are derived.

Introduction

The working principle of electrochemical machining (ECM) is based on the principle of anodic metal dissolution. It allows the machining of metallic materials regardless of their mechanical properties [1,2,4,5,6]. The removal properties of a material depend on the electrochemical interactions between the workpiece material and the electrolyte.

Currently, the design of the cathode geometry and the derivation of process parameters is challenging due to the material-dependent removal properties. Usually, the removal properties are determined by the user with the help of an empirical removal experiment series [2].

This paper presents the determination of the removal parameters of the hardened tool steel S390 [3]. The determination is done by applying the PECM variant of the ECM process. The PECM process differs from the ECM process in that an oscillating cathode and a pulsed direct current are applied.

Material

The tool steel S390 was selected as the anodic material. S390 is a powder metallurgical steel and was examined in a hardened heat treatment condition. The hardness was measured at 890 ±30 HV_{30}. Round samples with a diameter of 12 mm were selected for the experiments. The composition of the material is given by the manufacturer as follows: 67.46 % Fe, 1.64 % C, 0.60 % Si, 0.30 % Mn, 4.80 % Cr, 2.00 % Mo, 4.80 % V, 10.40 % W and 8.00 % Co [3]. The

initial surface was examined using a Hirox SEM SH-5500 scanning electron microscope (SEM) for SE and BSE images. These images are shown in Fig. 1.

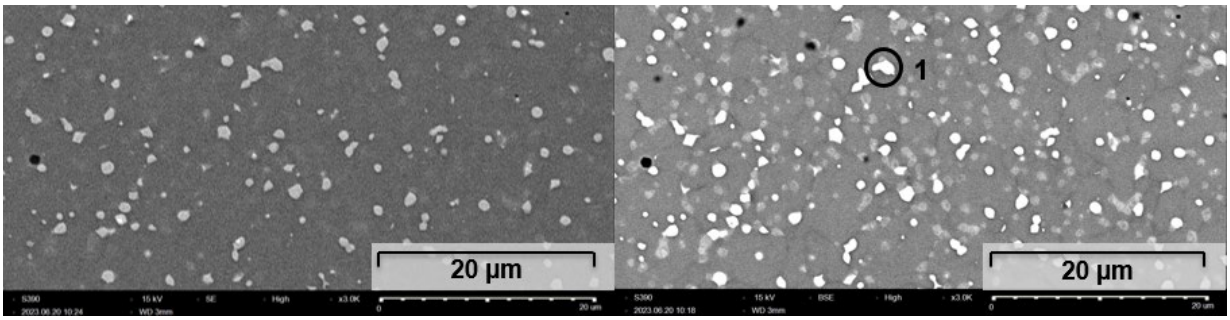

Figure 1: SEM image (left) and BSE image (right) of the base material

Several particles can be observed on the surface of the sample. The size of these particles varies between 0.5 µm and 2 µm. The main elements were determined by applying energy dispersive X-ray analysis (EDX) as follows: 46 % Fe, 29 % W and 11 % C. According to [7], these particles are comprised of Fe_3W_3C and VC carbides.

Experimental Setup

The experiments were conducted on a commercially available PEM 800S from PEMTec Snc. The design of the PECM device is based on DIN SPEC 91399 [4] and is shown in Fig. 2. A flushing chamber around the working gap encloses the cathode and anode. The flushing chamber channels the electrolyte, thus ensuring an exchange of the electrolyte and the removal of dissolved material. According to [4], the diameters of the cathode and anode are 12 mm, resulting in an effective removal area A_{sample} of 1.13 cm^2. The anode is made from 1.4301 (X5CrNi18-10).

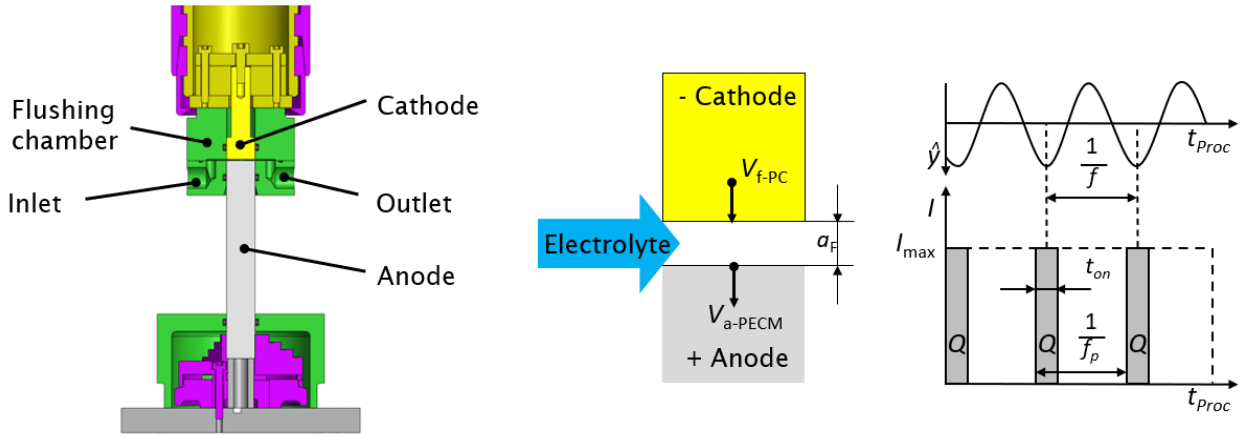

Figure 2: Schematic of the experimental setup (left) and schematic representation of removal and required current characteristics during the PECM process (right) according to [5]

In PECM, the cathode is oscillated, and therefore, the working distance is varied. In addition, in PECM, a pulsed direct current is applied. As shown in Fig. 2, the removal-effective current pulse is centered around the bottom dead center of the sine oscillation of the cathode. As a result, the working distance during the removal process is minimal. This ensures a high localization of the material removal. By opening the working gap and pausing the current, the working gap is more effectively flushed with fresh electrolyte, increasing the removal process's stability and reducing the working gap to up to 10 µm at the bottom dead center. [6]

Design of Experiments

The process parameters presented in Table 1 were kept constant over the various series of experiments. A $NaNO_3$ solution with an 8 % mass fraction was applied as an electrolyte. The specific removal volume V_{sp} was calculated as 2.495 e^{-5} cm^3/C based on the chemical composition. The oscillation frequency and the pulse frequency were set to 50 Hz. The pulse width was determined to be 4 ms.

Table 1: Constant parameters

Symbol	Parameter	Value
	Electrolyte $NaNO_3$	8 [% mass fraction]
σ	Electric conductivity	67 [mS/cm]
p_{el}	Electrolyte inlet pressure	350 [kPa]
f	Oscillation frequency	50 [Hz]
Z	Oscillation amplitude	200 [µm]
f_p	Pulse frequency	50 [Hz]
t_p	Pulse width	4 [ms]

Current densities J in the range from 2 A/cm^2 to 100 A/cm^2 were realized in the experiments. The aimed working distances were between 20 µm and 90 µm. For this purpose, the process input variables shown in Table 2 were varied in the specified ranges.

Table 2: Experimental parameters

Symbol	Parameter	Value Range
U_q	Voltage	5 – 18 [V]
v_f	Feed rate	0.002 – 0.321 [mm/min]

Experimental Results

After completion of the removal experiments, the optical appearance of the machined surfaces was analyzed. Fig. 3 shows the macroscopic surface appearance for different current densities. The working distance a_f was kept constant at 50 µm for each experiment. It can be observed that the surface appearance changes depending on the current density. The color change can be divided into three areas. A dark surface is observed in the range between 20 A/cm2 and 40 A/cm2. The samples ranging from 50 A/cm^2 to 67 A/cm^2 appear to have a reddish-gray surface. A slight metallic shine can be seen in some areas of the surface. Beginning with a current density of 80 A/cm^2, a shiny metallic surface is generated.

Another influencing factor is the flow direction of the electrolyte. The fresh electrolyte is fed into the working gap from the left and transported out on the right side. For samples with a current density above 50 A/cm^2, it can be seen that the surfaces in the area of the inlet show a metallic shine, which decreases in the direction of the electrolyte flow. This can be seen particularly clearly on the sample with a current density of 50 A/cm^2. The reason for this color change is the change in the electrolyte composition. The electrolyte is contaminated by the dissolution already taking place in the inlet area, which changes the removal conditions in the flow direction. This change in the electrolyte is reflected in the optical surface appearance.

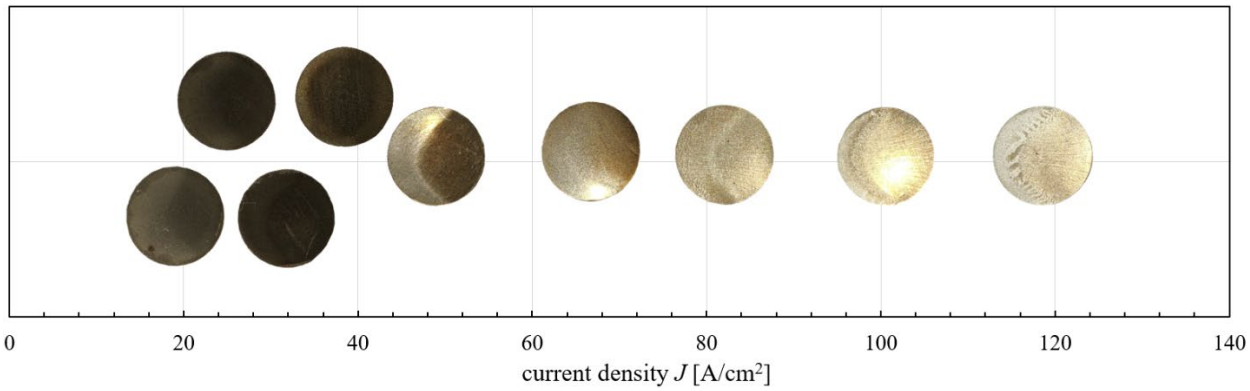

Figure 3: Photos of machined surfaces at different current densities J, constant working distance a_f of 50 µm

Fig. 4 shows the feed rate v_f of the cathode as a function of the current density J. The graph can be divided into three areas. Only minimal dissolution occurs in the range of low current densities below 30 A/cm2. The feed rate is near zero in this area (area 1). In the range from 33 A/cm^2 to 36 A/cm^2, a steep increase in the feed rate can be seen. For a current density higher than 38 A/cm^2, a linear increase with a lower gradient can be observed.

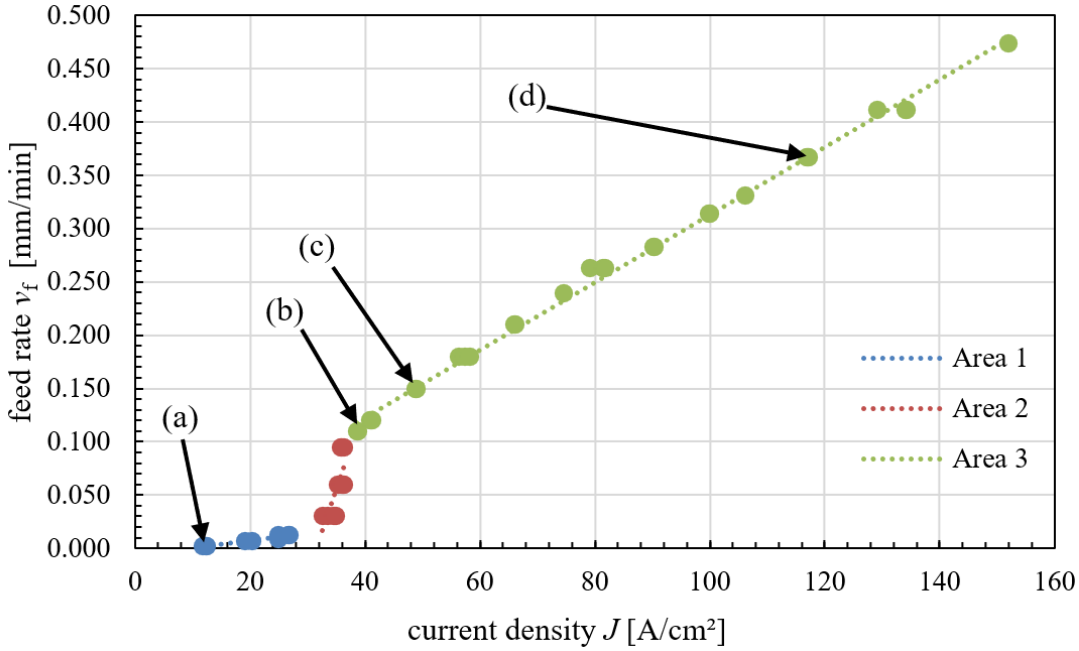

Figure 4: Feed rate v_f as a function of the current density for PECM with a frequency f of 50 Hz and a pulse width t_p of 4 ms

The functional relationship is described using linear functions in equation 1:

$$v_f = v_{a-PC} = \frac{\Delta v_{a-PC}}{\Delta J} \cdot J + v_0. \quad (1)$$

The parameters of these functions are listed in Table 3.

Table 3: Parameters for the different areas of the function $v_f(J)$

Area	J [A/cm^2]	$\Delta v_{a\text{-PC}}/\Delta J$ [mm/min / A/cm²]	v_0 [mm/min]
1	12 – 30	0.0007	-0.0066
2	33 – 36	0.0162	-0.5116
3	38 – 117	0.0033	-0.0093

As only minimal dissolution occurs up to a current density of 30 A/cm^2, the material dissolution in $NaNO_3$ solution is classified as trans-passive according to [6]. The surfaces of the samples after PECM were examined more closely by applying a scanning electron microscope (SEM). Fig. 5 shows the surfaces of 4 samples at a magnification of 3000. The data points are additionally labelled (a) to (d) in Fig. 4.

Surface (a) represents a surface after machining in the passive dissolution range. Surface (b) corresponds with machining in the transition area between passive and trans-passive dissolution. Surface (c) and surface (d) represent the trans-passive dissolution.

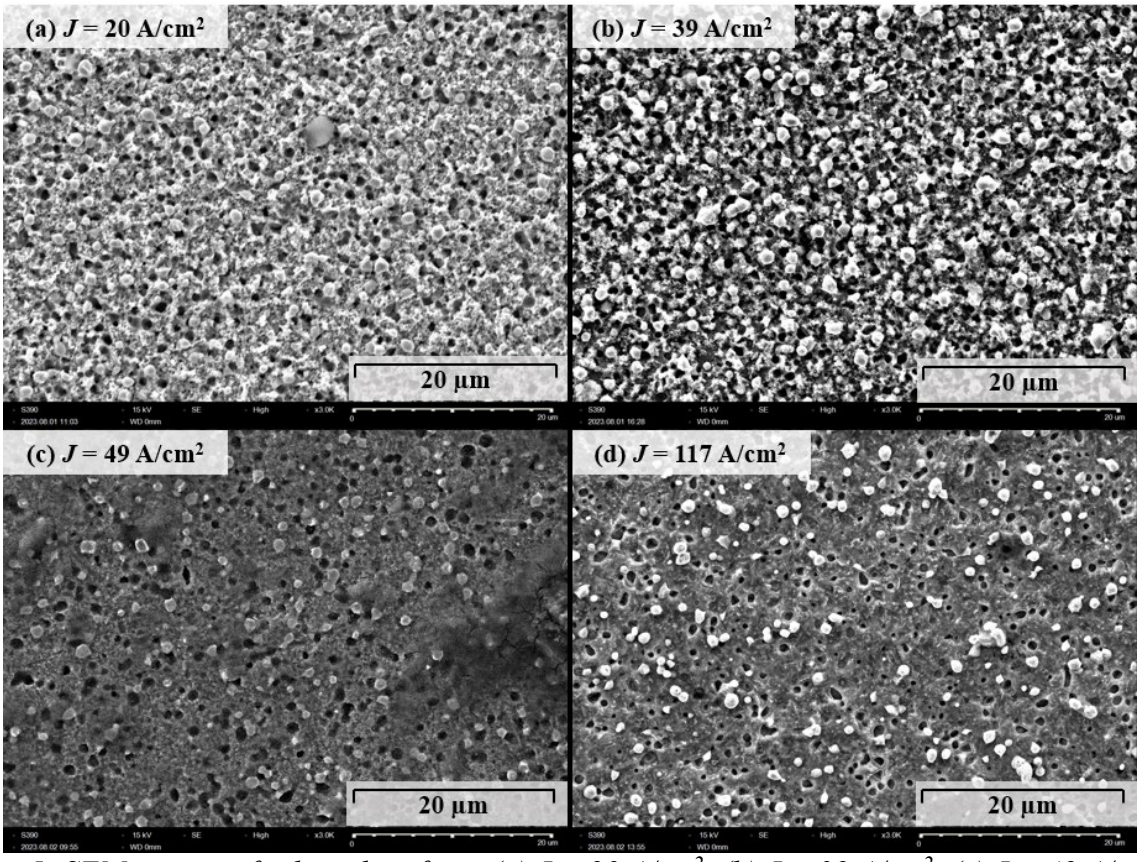

Figure 5: SEM images of selected surfaces (a) J = 20 A/cm^2, (b) J = 39 A/cm^2, (c) J = 49 A/cm^2, (d) J = 117 A/cm^2

When analyzing the SEM images, it is noticeable that the appearance of the surfaces changes significantly between samples which were machined with different current densities. The surface of the passive area (see Fig. 5(a)) has a fractured structure. Several of the particles already present on the initial surface can be recognized. These particles lie on a surface which appears porous. Surface (b) also shows the presence of numerous particles, but the surface seems less porous. Surface (c) represents the initial area of trans-passive dissolution. In contrast to (a) and (b), the

surface appears noticeably smoother and has only a few pores. As with the previous samples, the particles can also be seen on this sample surface. Sample (d) represents a surface machined with a high current density (J = 117 A/cm^2). The surface appears similar to the surface of sample (c).

All sample surfaces are covered with brightly highlighted particles. The particles are also present on the initial surface. The particles consist mainly of Fe (46 %), W (29 %) and C (11 %) and do not appear to be dissolved by anodic dissolution. Therefore, it can be assumed that these are covalent compounds of Fe_3W_3C and VC [7]. The pores, which can be seen in surfaces (c) and (d), are caused by particles that have already been loosened. It should be noted that although the particles themselves cannot be dissolved, they can be released from the material by dissolving the matrix material around them [8]. The particles are then transported by the flow of the electrolyte.

Fig. 6 shows the roughness *Sz* and the roughness *Sa* of the sample surface as a function of the current density *J*. The roughness values were determined by applying a Nanofocus µsurf expert. The measured data is processed by applying the factory settings with a 0.25 mm Gaussian filter. For each sample, three measurement squares were measured in the area of the inlet and the outlet. The roughness values are shown for the inlet and the outlet area. Furthermore, the arithmetic mean value formed from all six values is shown as the average roughness.

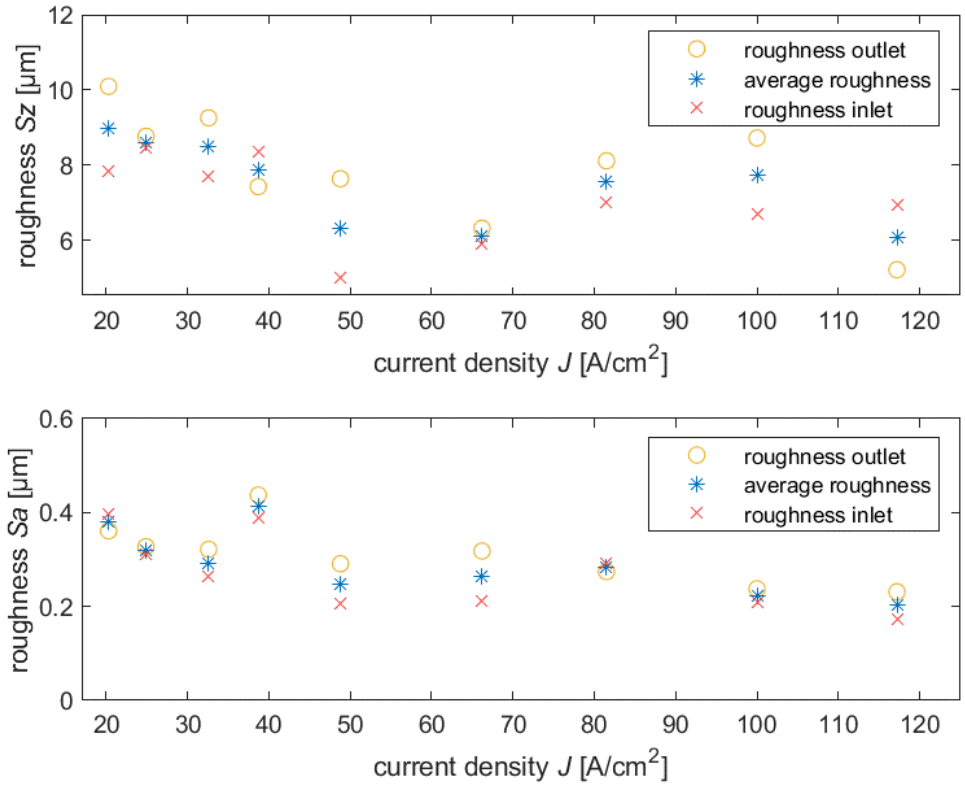

Figure 6: Surface roughness Sz and Sa as a function of the current density J

When looking at *Sz*, it is noticeable that the roughness decreases from *Sz* 9 µm at 20 A/cm^2 to *Sz* 6.1 µm and then rises slightly to a plateau of approx. *Sz* 7.5 µm at current densities between 80 A/cm^2 and 100 A/cm^2. Finally, the roughness falls again to a value of *Sz* 6 µm at 117 A/cm^2. The roughness *Sa* also decreases from 0.38 µm at 20 A/cm^2 to 0.21 µm at 50 A/cm^2. This trend is interrupted by the point of 0.42 µm at 38 A/cm^2. *Sa* then remains constant at around 0.21 µm. In the range around 50 A/cm^2 to 70 A/cm^2, a deviation of *Sa* between inlet and outlet of approx. 0.05 µm is noticeable. The deviations of *Sz* are larger than the deviations of *Sa* and scatter over the entire course between 0.3 µm at 25 A/cm^2 and 2.6 µm at 48 A/cm^2.

Fig. 7 shows the roughness values *Rz* and *Ra* in a similar format to Fig. 6. A line profile was evaluated for each of the previously analyzed measurement squares. Accordingly, 3 values are averaged in the inlet and outlet area. The *Rz* values initially fall from a roughness of 2.8 µm at 20 A/cm^2 to 1.4 µm at 66 A/cm^2. This trend is interrupted by the point at 40 A/cm^2 with 2.7 µm. In the range between 60 A/cm^2 and 117 A/cm^2, *Rz* is almost constant at 1.4 µm. The course of the roughness *Ra* is also decreasing and starts at 20 A/cm^2 with 0.3 µm. *Ra* falls on average to 0.19 µm at 50 A/cm^2. Like *Rz*, the graph of *Ra* also has a higher value at the point at 40 A/cm^2 with 0.31 µm. In the range between 50 A/cm^2 and 117 A/cm^2 *Ra* falls slightly from 0.19 µm to 0.13 µm. The differences between inlet and outlet are maximum for both *Rz* and *Ra* at 66 A/cm^2 with Δ*Rz* approx. 1.2 µm and Δ*Ra* approx. 0.13 µm. These differences decrease towards higher and lower current densities.

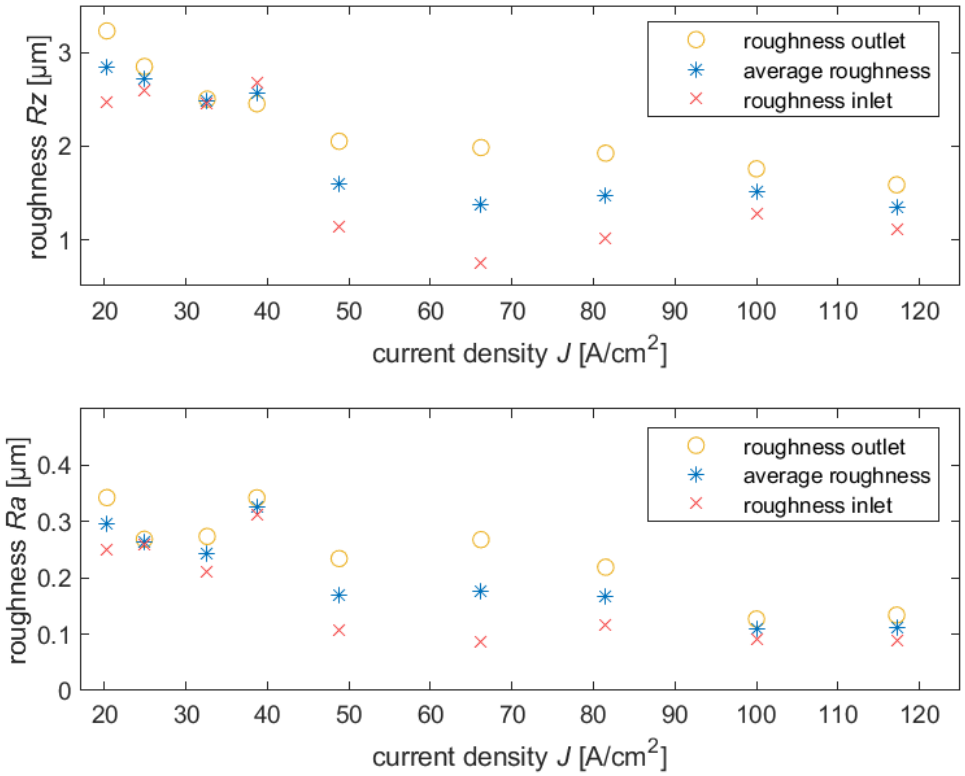

Figure 7: Roughness Rz and Ra as a function of the current density J

A comparison of the graphs from Fig. 6 and Fig. 7 shows that all graphs display a globally decreasing trend of the roughness with increasing current densities. This is consistent with the macroscopic (see Fig. 3) and microscopic (see Fig. 5) appearances. It is also noticeable that all graphs except *Sz* have a local maximum of 40 A/cm^2. Looking at the removal characteristics shown in Fig. 5, it is noticeable that these maxima match the transition area between the passive and the trans-passive removal areas. The microscopic surface structure (see Fig. 5(b)) also appears clearly fractured at this current density. This fractured structure particularly influences the roughness *Sa* and *Ra*, as these are based on the average profile height. The roughness *Sz* and *Rz*, which only consider the local distance between hill and valley, on the other hand, are less or not noticeably impacted by the fractured structure. It should also be noted that *Rz,* in particular, is subject to greater statistical fluctuation due to the presence of particles, as shown in Fig. 5. In general, the deviation of *Rz* and *Ra* values between inlet and outlet is maximum in the range of 50 A/cm^2 to 80 A/cm^2 and decreases towards higher and lower current densities.

Materials Research Proceedings 41 (2024) 2365-2373 https://doi.org/10.21741/9781644903131-260

Fig. 8 displays the current efficiency $\eta_{\text{v-a}}$ as a function of the current density J. The current efficiency $\eta_{\text{v-a}}$ is defined as the quotient of the effective removal volume V_{eff} and the specific removal volume V_{sp} according to equitation 2 [6]. The effective removal volume V_{eff} is calculated from the feed or removal rate v_{f} and the removal area A_{sample}.

$$\eta_{\text{v-a}} = \frac{V_{\text{eff}}}{V_{\text{sp}}} = \frac{v_{\text{f}} \cdot A_{\text{sample}}}{V_{\text{sp}}} \tag{2}$$

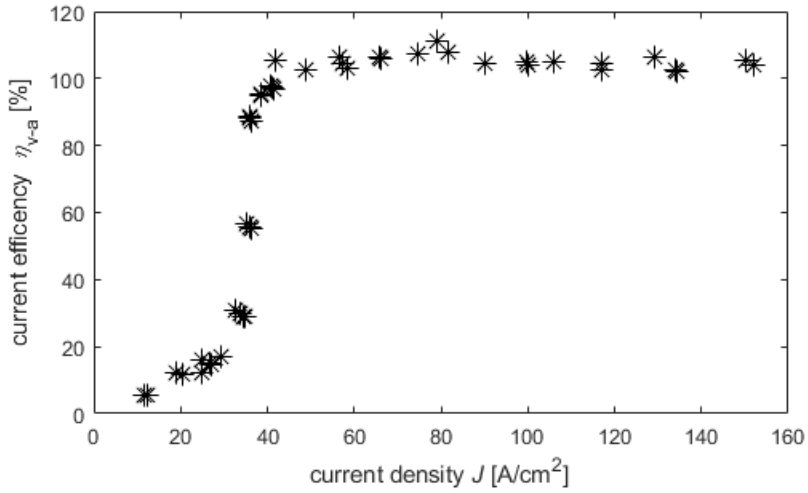

Figure 8: Current efficiency $\eta_{\text{v-a}}$ as a function of the current density J

It can be seen that the current efficiency in the range from 20 A/cm^2 to 40 A/cm^2 is below 20 % and increases slightly. Around 40 A/cm^2, the current efficiency jumps to a value between 100 % and 110 % and stays constant for rising current densities. The jump in the current efficiency is overlapped by the jump in the feed rate, as seen in Fig. 4. Usually, a current efficiency of 70 % to 80 % is to be expected for a material and electrolyte combination with trans-passive dissolution characteristics [8]. In the case of the analyzed material, however, it should be noted that the material is reinforced with covalent bonded particles. As mentioned, these particles are not dissolved anodically but instead drop out of the material when the matrix material around the particle is removed sufficiently. However, the volume of the particles is included in the removal volume of the current efficiency, which significantly increases the current efficiency.

As a result of this analysis, different process input parameters can be derived for the subsequent design of a PECM application for the machining of S390. It is to be noted that the following parameters and expected results only apply to parts and surfaces machined in the frontal working gap and application with sufficient flushing of electrolyte. The creation of current densities of 50 A/cm^2 up to 117 A/cm^2 results in a possible feed rate v_{f} of 0.15 mm/min up to 0.47 mm/min. The machined surfaces can be expected to have a roughness of *Rz* around 2 µm and below and *Ra* at 0.22 µm and below. A metallic shin of the machined surfaces can be expected. To reduce the machining time, a high current density and, therefore, a high feed rate is advised.

The creation of rougher and porous surfaces with *Rz* of 2.9 µm and *Ra* of 0.3 µm can be achieved using lower current densities below 35 A/cm^2. The machining with current densities below 35 A/cm^2 also creates a dark greyish surface appearance. Lower current densities, however, result in a low feed rate of 0.02 mm/min and lower, which increases the machining time. As these parameters only apply to machining in the frontal working gap, the usage of low current densities

for the creation of specific surfaces is advised only for surface finishing to avoid high machining time.

Summary

In this study, the removal characteristics of the hardened tool steel S390 under PECM conditions were investigated according to DIN SPEC 91399. The material dissolution was found to be trans-passive starting at a current density *J* of approx. 33 A/cm^2. During this investigation, the material removal was characterized by a pulse width of 4 ms. It could be shown that three linear functions describe the feed rate vf as a function of the current density *J.* Furthermore, the machined surfaces were examined macroscopically and microscopically. In addition, the roughness of the individual samples was examined for different current densities. A minimal roughness of *Rz* 1.36 µm and *Ra* 0.109 µm is achieved. Finally, the current efficiency was calculated.

Acknowledgements

The project work was funded by the Forschungsvereinigung Antriebstechnik e. V. with project number 986-I. The machine tool PEM 800S was funded by the German Research Foundation (DFG) with project number 467011871.

References

[1] J.F. Wilson: Practice and Theory of Electrochemical Machining. New York: Wiley-Interscience, 1971, ISBN 9780471949701

[2] G. Meichsner, M. Hackert-Oschätzchen, M. Krönert, J. Edelmann, A. Schubert, M. Putz, Fast Determination of the Material Removal Characteristics in Pulsed Electrochemical Machining, Procedia CIRP 46 (2016) 123-126. https://doi.org/10.1016/j.procir.2016.03.175

[3] N.N., SCHNELLARBEITSSTÄHLE- BÖHLER S390 MICROCLEA, Datasheet, URL: https://www.bohler.de/app/uploads/sites/92/2023/08/productdb/api/s390-microclean_de.pdf, last checked 20.12.2023

[4] DIN SPEC 91399 - Method for determining process input parameters for precision electrochemical machining – requirements, criteria, definitions. Berlin: Beuth Verlag, 2018. https://dx.doi.org/10.31030/3007935

[5] G. Meichsner, M. Hackert-Oschätzchen, T. Petzold, M. Krönert, J. Edelmann, A. Schubert, M. Putz, Removal Characteristics of Stainless Steel in Pulsed Electrochemical Machining, in 12th International Symposium on Electrochemical Machining Technology, INSECT 2016 Proceedings, Brussels, 2016, 73-83. ISBN 978-9-4619746-1-7

[6] F. Klocke, W. Koenig.: Fertigungsverfahren Band 3. Springer Verlag, 2007. https://doi.org/10.1007/978-3-540-48954-2

[7] H. Peng, L. Hu, L. Li, L. Zhang, X. Zhang, Evolution of the microstructure and mechanical properties of powder metallurgical high-speed steel S390 after heat treatment, Journal of Alloys and Compounds 740 (2018) 766-773. https://doi.org/10.1016/j.jallcom.2017.12.264

[8] T. Haisch, E. Mittemeijer, J.W. Schultze, Electrochemical machining of the steel 100Cr6 in aqueous NaCl and NaNO3 solutions in the microstructure of surface films formed by carbides, Electrochimica Acta 47 (2001) 235–241. https://doi.org/10.1016/S0013-4686(01)00561-8